Journal of Virology

The M, E, and N Structural Proteins of the Severe Acute Respiratory Syndrome Coronavirus Are Required for Efficient Assembly, Trafficking, and Release of Virus-Like Particles

Y. L. Siu, K. T. Teoh, J. Lo, C. M. Chan, F. Kien, N. Escriou, S. W. Tsao, J. M. Nicholls, R. Altmeyer, J. S. M. Peiris, R. Bruzzone and B. Nal

J. Virol. **2008, 82(22):11318. DOI: 10.1128/JVI.01052-08. Published Ahead of Print 27 August 2008.**

JOURNAL OF VIROLOGY, Nov. 2008, p. 11318–11330 Vol. 82, No. 22
0022-538X/08/$08.00+0 doi:10.1128/JVI.01052-08

The M, E, and N Structural Proteins of the Severe Acute Respiratory Syndrome Coronavirus Are Required for Efficient Assembly, Trafficking, and Release of Virus-Like Particles▽†

Y. L. Siu,[1] K. T. Teoh,[1] J. Lo,[2] C. M. Chan,[3] F. Kien,[1] N. Escriou,[4] S. W. Tsao,[5] J. M. Nicholls,[2] R. Altmeyer,[6] J. S. M. Peiris,[1,3] R. Bruzzone,[1] and B. Nal[1]*

HKU-Pasteur Research Centre, 8 Sassoon Road, Hong Kong SAR, China[1]; Department of Pathology, The University of Hong Kong, Queen Mary Hospital, Hong Kong SAR, China[2]; Department of Microbiology, The University of Hong Kong, 21 Sassoon Road, Hong Kong SAR, China[3]; Institut Pasteur, Unité de Génétique Moléculaire des Virus Respiratoires, URA-CNRS 3015, 25-28 Rue du Docteur Roux, 75724 Paris Cedex 15, France[4]; Department of Anatomy, The University of Hong Kong, 21 Sassoon Road, Hong Kong SAR, China[5]; and CombinatoRx-Singapore Pte, Ltd., 11 Biopolis Way, 138667 Singapore[6]

Received 20 May 2008/Accepted 7 August 2008

The production of virus-like particles (VLPs) constitutes a relevant and safe model to study molecular determinants of virion egress. The minimal requirement for the assembly of VLPs for the coronavirus responsible for severe acute respiratory syndrome in humans (SARS-CoV) is still controversial. Recent studies have shown that SARS-CoV VLP formation depends on either M and E proteins or M and N proteins. Here we show that both E and N proteins must be coexpressed with M protein for the efficient production and release of VLPs by transfected Vero E6 cells. This suggests that the mechanism of SARS-CoV assembly differs from that of other studied coronaviruses, which only require M and E proteins for VLP formation. When coexpressed, the native envelope trimeric S glycoprotein is incorporated onto VLPs. Interestingly, when a fluorescent protein tag is added to the C-terminal end of N or S protein, but not M protein, the chimeric viral proteins can be assembled within VLPs and allow visualization of VLP production and trafficking in living cells by state-of-the-art imaging technologies. Fluorescent VLPs will be used further to investigate the role of cellular machineries during SARS-CoV egress.

Coronaviruses are positive-sense RNA enveloped viruses that belong to the *Coronaviridae* family in the *Nidovirales* order. These viruses are found in a wide variety of animals and can cause respiratory and enteric disorders of diverse severity (11, 18). In the past 5 years, several human and animal coronaviruses have been discovered, including the highly pathogenic virus responsible for the severe acute respiratory syndrome (SARS-CoV) (34, 58, 60, 64, 68, 69). Coronavirus particles consist of a helical nucleocapsid structure, formed by the association between nucleocapsid (N) phosphoproteins and the viral genomic RNA, which is surrounded by a lipid bilayer where three or four types of structural proteins are inserted: the spike (S), the membrane (M), and the envelope (E) proteins and, for some coronaviruses only, the hemagglutinin-esterase (HE) protein (for a review, see reference 14). Once sufficient amounts of new genomic RNA and structural proteins have been produced, assembly of particles occurs. Assembly and release of virions are the last stages of the virus life cycle.

The triple-spanning membrane glycoprotein M drives the assembly of coronavirus, which bud into the lumen of the endoplasmic reticulum-Golgi intermediary compartment (ERGIC) (32, 33, 62, 63). M is the most abundant envelope protein that sorts viral components to be incorporated into virions. M oligomerization, mainly driven by its transmembrane domain, is believed to allow the formation of a lattice of M proteins at ERGIC membranes (16, 41). S and E membrane proteins are integrated into the lattice through lateral interactions with M, whereas N and viral RNA interact with M C-terminal domain, which is exposed to the cytosol (4, 8, 15, 19, 30, 36, 48, 54, 55). The coronavirus S protein, responsible for receptor binding and membrane fusion, does not seem to have any major role in coronavirus assembly. Recent studies show that E is a viroporin that forms ion channels (46, 66, 67). Despite its minor incorporation into virion particles (7, 22, 40), the small E protein plays an important but not fully understood role in virus morphogenesis and budding (20, 35, 70). Studies performed on coronaviruses, including the SARS-CoV, demonstrate that depletion of the E gene from coronavirus genome strongly diminish virus growth and particle formation (9, 12, 35, 37, 57). The N protein self-associates and encapsidates the RNA genome for incorporation into budding virions through interactions with the M protein independently of E and S proteins (24, 52, 53, 61). For SARS-CoV, the interaction of N with M was described to be independent of viral RNA (25, 45).

Work on mouse hepatitis virus (MHV), bovine coronavirus, infectious bronchitis virus, and transmissible gastroenteritis virus has established that E and M proteins are necessary and sufficient for assembly of virus-like particles (VLPs), which share size and morphological features with real viruses (1, 2, 7, 8, 38, 65). Nevertheless, the minimal requirement for assembly of SARS-CoV VLPs is still controversial. Y. Huang et al. described formation of VLPs in transfected human 293 renal

* Corresponding author. Mailing address: HKU-Pasteur Research Centre, 8 Sassoon Road, Hong Kong SAR, China. Phone: (852) 2816-8403. Fax: (852) 2872-5782. E-mail: bnal@hku.hk.

† Supplemental material for this article may be found at http://jvi.asm.org/.

▽ Published ahead of print on 27 August 2008.

epithelial cells that only required coexpression of the M and N viral proteins (29). On the contrary, other studies described that coexpressed M and E proteins were sufficient for release of sedimentable particles from transfected mammalian cells (27) or insect cells, using a baculovirus expression system (26, 50). A few groups have proposed immunization with SARS-CoV VLPs as an effective vaccine strategy. VLPs produced in insect cells or chimeric MHV/SARS-CoV VLPs produced in mammalian cells were used in these studies (42, 44).

Our objective was to delineate the molecular mechanisms that regulate SARS-CoV egress in mammalian cells. Here we demonstrate that whereas VLPs could hardly be recovered from culture medium of cells coexpressing combinations of M and E or M and N proteins, coexpression of both SARS-CoV E and N with M allowed the release of significant levels of VLPs within 1 day. When coexpressed, the trimeric S protein was found in VLPs. Therefore, in apparent contrast to other coronaviruses, SARS-CoV egress strongly depends on three structural proteins: M, E, and N. The addition of fluorescent tags to viral structural proteins allowed us to visualize the egress of fluorescent VLPs in living cells. Monitoring of VLP egress in living cells will be a powerful new tool for studying the involvement of viral and cellular factors during the late stages of the SARS-CoV life cycle.

MATERIALS AND METHODS

Cells and culture conditions. The Vero E6 African green Monkey kidney cell line was cultured in Dulbecco modified Eagle medium (DMEM) supplemented with 10% heat-inactivated fetal calf serum, 100 U of penicillin, and 100 μg of streptomycin per ml at 37°C with 5% CO_2.

Plasmid constructions. cDNAs coding for the SARS-CoV M, E, S, and N structural proteins were codon optimized for mammalian cells and synthesized by GeneArt (Regensburg, Germany). The M cDNA was amplified by PCR and subcloned into the pIRES plasmid vector (BD Biosciences, San Jose, CA) between the NheI and EcoR I restriction sites of the upstream multiple cloning site. The E cDNA was amplified by PCR and inserted either into the pcDNA3.1 plasmid vector between the KpnI and NotI restriction sites or into the pIRES plasmid vector between the SalI and NotI restriction sites of the downstream multiple cloning site. The S cDNA was amplified by PCR and inserted either into the pcDNA3.1 plasmid vector between the NheI and ApaI restriction sites. The pcDNA-Nflag plasmid was constructed from the original pCRScript-Nflag (produced by GeneArt, Regensburg, Germany) using the KpnI and XhoI restriction sites. The Flag tag was in fusion with the 3′ end of N cDNA and separated from N cDNA by six nucleotides encoding two glycine residues. The cDNAs coding for the enhanced yellow (eYFP), cyan (eCFP), and green (eGFP) fluorescent proteins and the monomeric red fluorescent protein (mRFP1) (5) were amplified by PCR from plasmids purchased from Clontech Laboratories (Takara Bio, Shiga, Japan) and subcloned into pcDNA3.1 or pIRES vectors. The S, N, or M cDNAs were then inserted 5′ to the fluorescent protein cDNAs using the ClaI and ApaI sites (S and N) or the XhoI and MluI (M) restriction sites. The two fused cDNAs were separated by two codons encoding glycines.

Antibodies. The M and E proteins were detected with rabbit polyclonal antibodies raised against the C-terminal extremity of each protein. The rabbit polyclonal antibody against the M C-terminal domain was purchased from ProSci, Inc. (Poway, CA). The rabbit polyclonal antibody against the E protein was produced by Nicolas Escriou (Institut Pasteur, Paris, France) using a C-terminal peptide. The Flag tag was detected with the mouse monoclonal immunoglobulin G1 M2 antibody purchased from Sigma-Aldrich. The mouse polyclonal antibody against the S protein was obtained by immunizing mice with purified S trimers expressed in mammalian cells as described previously (31). The mouse monoclonal antibody against the N protein was a generous gift from K. H. Chan (Department of Microbiology, University of Hong Kong) and produced as described previously (56).

Transient transfections and production of SARS-CoV VLPs. A total of 8×10^5 cells were plated in 75-cm^2 dishes, incubated overnight, and transfected with plasmid constructs using a FuGENE 6 transfection reagent (Roche, Basel, Switzerland), according to the manufacturer's instructions. Briefly, 54 μl of FuGENE 6 transfection reagent was mixed with DMEM, followed by incubation for 5 min, and then 6 μg of each plasmid was added. The FuGENE 6-plasmid mixture was incubated for 30 min at room temperature. Cell medium was discarded and replaced with 3 ml of warm DMEM. The FuGENE 6-plasmid mixture was added to the cells. After 3 h of incubation at 37°C, the medium containing the transfection mixture was discarded, and 10 ml of fresh medium was added. Cells were incubated for 21 or 45 h.

Purification of SARS-CoV VLPs. At 24 or 48 h posttransfection, cell medium was collected and cleared by centrifugation at low speed (1,000 × *g* for 10 min) to pull down cell debris. After passage through 0.45-μm-pore-size filter, cleared cell medium was then loaded on top of 20% sucrose cushions and ultracentrifuged for 3 h at 28,000 rpm using a SW41 rotor (Belkman Coulter, Inc., Fullerton, CA). VLP-containing pellets were resuspended in TNE buffer (50 mM Tris-HCl, 100 mM NaCl, 0.5 mM EDTA, [pH 7.4]).

Western blot analysis of VLPs and cell lysates. For Western blot analysis of purified VLPs, 15 μl of resuspended pellets from ultracentrifuged culture medium was mixed with 5 μl of lithium dodecyl sulfate-containing loading buffer and loaded onto 4 to 12% polyacrylamide gels (NuPAGE Novex Bis-Tris Mini Gels; Invitrogen, Carlsbad, CA). Electrophoresis was performed with the NuPAGE morpholinepropanesulfonic acid sodium dodecyl sulfate (SDS) running buffer from the same manufacturer. Alternatively, resuspended pellets from 48-h time points were loaded on top of 20 to 60% sucrose gradients and ultracentrifuged for 3.5 h at 26,700 rpm (27). Twenty fractions were collected and analyzed by Western blotting. For Western blot analysis of cell lysates, cells were washed twice with 1× phosphate-buffered saline (PBS) at 24 or 48 h posttransfection and lysed in lysis buffer containing 1% Triton X-100, 150 mM NaCl, 20 mM Tris-HCl (pH 7.5), and 1 mM EDTA for 15 min on ice with frequent vortexing. The lysates were then cleared by centrifugation at 16,100 × *g* for 15 min at 4°C and analyzed by Western blotting. Next, 15 μl of each lysate was mixed with 5 μl of lithium dodecyl sulfate loading buffer and loaded on polyacrylamide gels. For detection of E but not S, samples were treated with dithiothreitol and heated at 95°C for 5 min before migration on polyacrylamide gels. To detect both E and trimers of S from same preparations, samples were split and either treated or not treated before loading of two separate gels for E and S detection, respectively. The results for M and Nflag were similar with or without treatment.

Electron microscopy. For transmission electron microscopy experiments, transfected cells were harvested at 24 and 48 h posttransfection. Cells were detached using 10 mM EDTA, fixed in 2.5% glutaraldehyde in cacodylate buffer, and postfixed with 1% osmium tetroxide (OsO_4) in cacodylate buffer for 1 h at room temperature. The cells were then embedded in 2% agarose to form cell blocks that were dehydrated in graded series of ethanol and embedded in epoxy resin. Ultrathin sections were stained for 45 min with 2% aqueous uranyl acetate and for 30 min with Reynolds lead citrate. For analysis of secreted VLPs, the VLPs were purified from the cell medium by ultracentrifugation on a 20% sucrose cushion and separated on a 20 to 60% discontinuous sucrose gradient, and fraction 10 was collected and then concentrated by ultracentrifugation in TNE buffer (pH 7.4) for 1 h at 28,000 rpm. Next, 5 μl of the VLP suspension, mixed with an equal volume of negative stain (2% aqueous uranyl acetate and 2% phosphotungstate solution [pH 7.0]), was placed onto a Formvar-carbon-coated copper grid for 2 min, and the excess suspension was drained. The grids were viewed and photographed with a Philip CM100 electron microscope at 80 kV.

Fluorescence microscopy. For fluorescence microscopy on fixed cells, Vero E6 cells were grown on glass coverslips, transfected, and analyzed at 24 h posttransfection. Cells were washed with PBS, nuclei were stained with DAPI (4′,6′-diamidino-2-phenylindole), and coverslips were mounted on glass slides for analysis. Fixed cells were visualized under an AxioObserver Z1 inverted motorized fluorescence microscope using the ApoTome module and piloted through the Axiovision 4.6 software, and images were acquired through an MRm AxioCam high-resolution charge-coupled device camera (Carl Zeiss, Germany). For fluorescence microscopy on live cells, Vero E6 cells were grown in a glass-bottom culture dish (MatTech), transfected, and analyzed at 24 h posttransfection. The cells were washed, and the medium was changed to Hanks balanced salt solution-OptiMEM prewarmed culture medium. Wide-field image acquisitions of live cells were obtained using the system described above. Confocal acquisitions of live cells were acquired at the Hong Kong University Core Imaging Facility using an AxioObserver Z1 inverted motorized fluorescence microscope equipped with a spinning disc confocal imaging system (UltraVIEW ERS; Perkin-Elmer, Shelton, CT). For brefeldin A (BFA) treatment, cells were incubated with 6 μg per ml of BFA for the indicated times. To release the BFA effect, the cells were washed three times in 1× PBS and reincubated in normal medium for the indicated times.

RESULTS

Efficient production and release of SARS-CoV VLPs are driven by coexpression of M, N, and E structural proteins. To determine the optimal conditions for efficient SARS-CoV VLP production, we chose to coexpress different combinations of structural proteins in the Vero E6 African green monkey cell line, which is permissive to SARS-CoV replication (34). cDNAs encoding SARS-CoV structural proteins M, E, and N were codon optimized for expression in mammalian cells. Understanding the importance of maintaining a low E/M ratio in transfected cells to ensure low incorporation of E into VLPs and to prevent the potential formation of E-containing vesicles, we reasoned that the use of the pIRES bicistronic plasmid should be appropriate. This plasmid presents the double advantage to ensure coexpression of both cDNAs in transfected cell and allows a reduced rate of translation of the downstream gene by utilizing a partially disabled internal ribosome entry site (IRES) sequence. We therefore subcloned M upstream of E cDNA in the pIRES vector. N was expressed from a pcDNA plasmid with a C-terminal Flag tag. Vero E6 cells were either not transfected or transfected with pcDNA-E, pIRES-M, or pIRES-M-E alone, pIRES-M plus pcDNA-Nflag, and pIRES-M-E plus pcDNA-Nflag (Fig. 1A). At 24 and 48 h posttransfection, the culture medium and cells were harvested. The culture medium was subjected to ultracentrifugation on a 20% sucrose cushion to isolate VLPs, and the SARS-CoV structural proteins assembled into VLPs were analyzed by Western blotting.

The M protein was readily detected at both 24 and 48 h posttransfection in lysates from Vero E6 cells transfected with pIRES-M, pIRES-M-E, pIRES-M plus pcDNA-Nflag, and pIRES-M-E plus pcDNA-Nflag (Fig. 1A, upper panels). As described previously, three major forms of M, which correspond to different glycoforms, were detected by SDS-polyacrylamide gel electrophoresis: two bands at ca. 18 and 28 kDa and a smear at higher molecular sizes reflecting heterogeneity of glycosylation patterns (51). As expected, higher levels of M were detected in cell lysates at 48 h than at 24 h posttransfection. Whereas a 10-kDa protein corresponding to E could be easily detected in cell lysates from cells transfected with pcDNA-E plasmid, its expression was much lower in cells transfected with the pIRES-M-E bicistronic vector. The Nflag protein was found in cell lysates from both pIRES-M plus pcDNA-Nflag and pIRES-M-E plus pcDNA-Nflag transfected cells at similar levels. A major band corresponding to a protein with an apparent molecular size of 45 kDa was detected.

Strikingly, the efficacy of VLP production was dramatically affected by the combination of viral proteins coexpressed (Fig. 1A, lower panels). Although M was not detected in ultracentrifuged culture medium from pIRES-M, pIRES-M-E, or pIRES-M plus pcDNA-Nflag transfected cells at 24 h posttransfection, significant levels were found in preparations from pIRES-M-E plus pcDNA-Nflag transfected cells. Similarly, the N protein was only detected in ultracentrifuged culture medium from pIRES-M-E plus pcDNA-Nflag transfected cells at this early time point. Signals for E were below the limit of detection at 24 h and detectable only at 48 h. Finding low amounts of E in VLPs is in accordance with the minor presence of this protein in coronavirus particles, despite its important role for virion assembly and budding (9, 20, 37, 57, 65). In conclusion, only when M, E, and N proteins were coexpressed, VLPs that contained the M and N proteins could be isolated from the culture medium at 24 h posttransfection.

At 48 h posttransfection, E was found in ultracentrifuged culture medium from cells transfected with the pcDNA-E plasmid alone. This is in agreement with previously published data that describe secretion of E proteins independently of other viral elements (7, 47, 50). At this time point, trace amounts of M were detected in ultracentrifuged culture medium from pIRES-M and pIRES-M-E transfected cells, whereas significant levels of M and N were found in pIRES-M plus pcDNA-Nflag ultracentrifuged culture medium. Independent secretion of SARS-CoV M proteins from Vero E6 cells as well as production of M-E VLPs was described by Mortola and Roy (50) at 4 days posttransfection. The production of SARS-CoV M-N VLPs has already been reported by Y. Huang et al. in transfected 293 renal epithelial cells at 63 h posttransfection (29). Very interestingly, in the conditions described here, significantly higher levels of M and N proteins were found in purified VLPs from pIRES-M-E plus pcDNA-Nflag than in those from pIRES-M plus pcDNA-Nflag transfected cells at 48 h posttransfection. We were also able to detect E in these conditions, but not when cells were only transfected with the pIRES-M-E vector.

In order to verify that inefficacy of production of M-E VLPs by cells transfected with pIRES-M-E was not due to inefficient E expression, we performed similar experiments but expressed E from a pCDNA-E plasmid and analyzed cells and medium at 48 h posttransfection (Fig. 1B). As expected, higher levels of E were detected in the lysates of cells transfected with pIRES-M plus pCDNA-E and with pIRES-M plus pCDNA-E plus pCDNA-Nflag than in the lysates of cells transfected with pIRES-M-E and with pIRES-M-E plus pCDNA-Nflag, respectively (Fig. 1B, left panel). Nevertheless, neither production of M-E VLPs nor production of M-E-N VLPs was improved by an increase in E expression (Fig. 1B, right panel). On the contrary, production of M-E-N VLPs was enhanced when the bicistronic vector was used, as indicated by higher levels of Nflag, M, and E proteins secreted, and the ratio E(medium)/E(lysate) was significantly higher in these conditions. This result suggests that expression of E along with M from the pIRES-M-E bicistronic vector and in combination with N favors the production of SARS-CoV VLPs.

We then investigated cosedimentation of secreted viral structural proteins by performing sucrose gradient fractionation on ultracentrifuged cell medium. Cells were either transfected by individual plasmids or combinations of plasmids as described previously. In this experiment we used the individual plasmid for E expression to verify the potential presence of E-containing vesicles in medium when E was expressed at higher levels. At 48 h posttransfection, cleared cell medium was ultracentrifuged on 20% sucrose cushion, and pellets were resuspended in TNE buffer. As controls, viral proteins contained in cell lysates and pellets from ultracentrifuged medium were analyzed by Western blotting (Fig. 1C, left panel). Pellets were loaded on top of 20 to 60% discontinuous sucrose gradients. After another round of ultracentrifugation, 20 fractions were collected and analyzed by Western blotting (Fig. 1C, right panels a to e). The results were consistent with the data de-

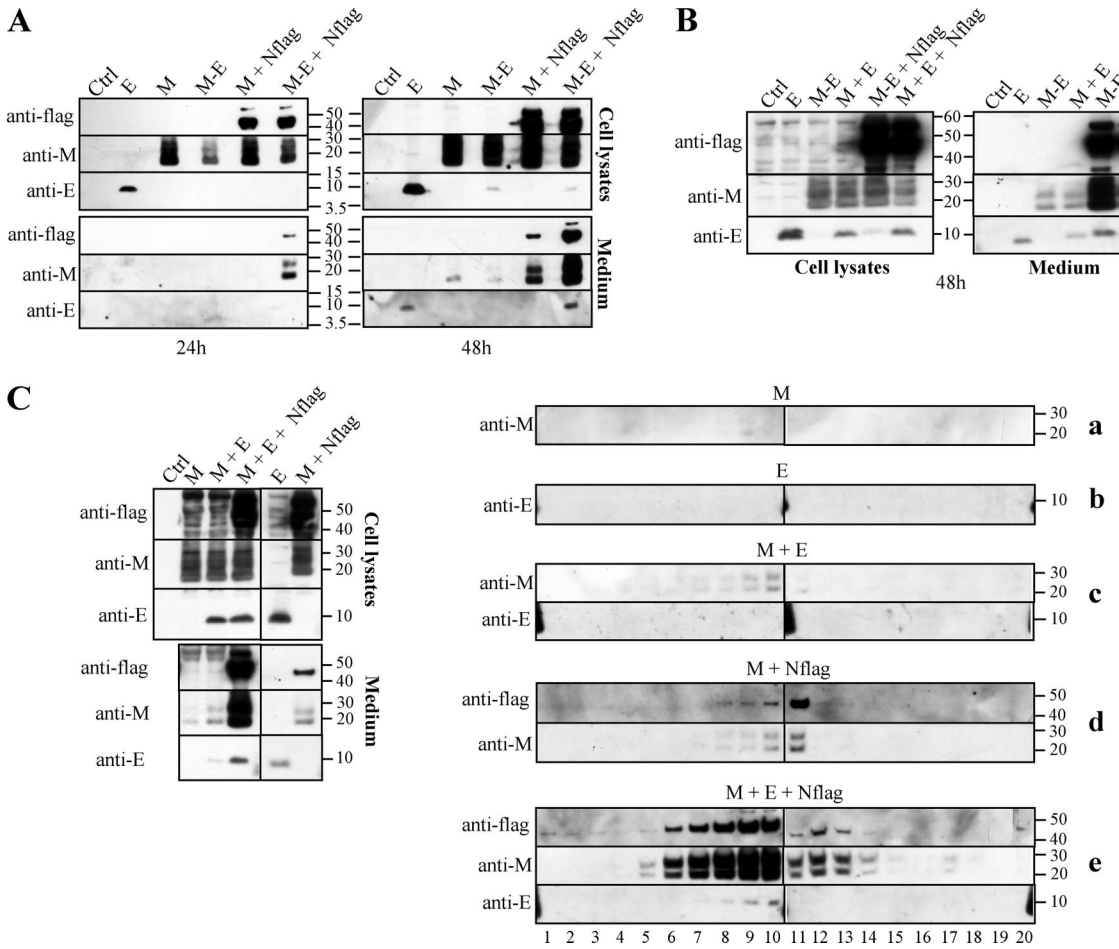

FIG. 1. Production of SARS-CoV VLPs by transfected Vero E6 cells. (A) Coexpression of M, E, and N is necessary for efficient secretion of SARS-CoV VLPs by Vero E6 cells at 24 and 48 h posttransfection. Monolayers of Vero E6 cells were transfected with plasmids driving the expression of the SARS-CoV structural proteins M, E, and Flag-tagged N as specified at the top of each lane. Protein expression in cell lysates and in VLPs isolated from culture medium was analyzed by Western blotting at 24 and 48 h posttransfection, as indicated below the corresponding panels. Samples were heat denatured and reduced with dithiothreitol before loading. The M and E proteins were detected with rabbit polyclonal antibodies produced against the C-terminal extremity of each proteins. The N protein was detected with the M2 monoclonal antibody recognizing the Flag tag. Blots were exposed for 1 min for signal detection except for the detection of E contained in pellets from ultracentrifuged culture medium (bottom panels), for which blots were exposed for 10 min. The molecular mass (in kilodaltons) and the migration of protein standards are shown between the blots. (B) Use of the bicistronic pIRES-M-E vector restrains the E expression level and favors the production of M-E-N VLPs. Vero E6 cells were transfected with the indicated plasmid combinations, and the cell lysates and medium were analyzed at 48 h posttransfection as in panel A. To ensure better detection of E, VLPs were concentrated four times more than in panel A. Blots were exposed for 10 s for signal detection except for the detection of E contained in pellets from ultracentrifuged culture medium (right bottom panel), for which the blot was exposed for 1 min. (C) Secreted viral structural proteins cosediment in sucrose gradient. Three 75-cm^2 dishes of Vero E6 cells were transfected with plasmids driving the expression of SARS-CoV structural proteins M, E, and Flag-tagged N either individually or in combination. Protein expression in cell lysates and in pellets from culture medium ultracentrifuged on 20% sucrose cushion was controlled by Western blot at 48 h posttransfection (left panel). Resuspended pellets from ultracentrifuged cell medium were then loaded on a 20 to 60% discontinuous sucrose gradient and subjected to fractionation by ultracentrifugation. Twenty fractions of 600 μl were collected (1 to 20, from lightest to heaviest). The nature of viral proteins associated with each fraction was determined by Western blotting (a to e). Portions (15 μl) of samples were heat denatured and reduced with dithiothreitol before loading. The molecular mass (in kilodaltons) and the migration of protein standards are shown on the right sides of the blots. Samples from (i) pIRES-M, pIRES-M plus pCDNA-E, and pIRES-M plus pCDNA-E plus pcDNA-Nflag and (ii) pcDNA-E and pIRES-M plus pcDNA-Nflag were generated in two separate experiments. Ctrl, nontransfected cells; E, pCDNA-E; M, pIRES-M; M-E, pIRES-M-E; M + Nflag, pIRES-M plus pcDNA-Nflag; M-E + Nflag, pIRES-M-E plus pcDNA-Nflag; M + E, pIRES-M + pcDNA-E; M + E + Nflag, pIRES-M plus pcDNA-E plus pcDNA-Nflag.

scribed in Fig. 1A and B. When M was expressed alone, very little protein was found in the cell medium, and traces were detected in fraction 9 (Fig.1Ca). Coexpression with E or Nflag allowed the secretion of slightly higher levels of M in cell medium and the detection of M in fractions 7 to 11, with enrichment in fraction 10 (Fig.1Cc) or 11 (Fig.1Cd), respectively. E protein was not detectable in fractions from the medium of either pCDNA-E or pIRES-M plus pCDNA-E transfected cells (Fig. 1Cb and c). Nflag cosedimented with M when coexpressed (Fig.1Cd). As expected, greater levels of M, E, and Nflag proteins were found in the medium from cells expressing all three viral proteins (Fig.1Ce). M and Nflag were

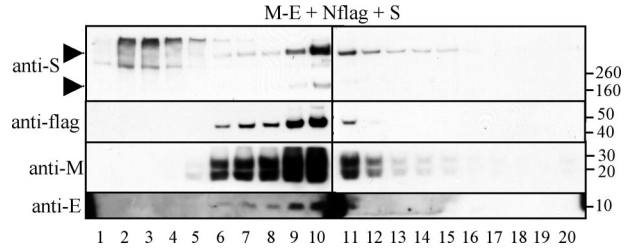

FIG. 2. S-glycoprotein trimers are incorporated onto SARS-CoV M, E, and N-containing VLPs. pcDNA-S plasmid was cotransfected with pIRES-M-E and pcDNA-Nflag vectors. The culture medium was harvested at 48 h posttransfection and ultracentrifuged on 20% sucrose cushion, and the pellets were resuspended in TNE buffer and ultracentrifuged on a 20 to 60% discontinuous sucrose gradient. Twenty fractions were collected (1 to 20, from lightest to heaviest) and analyzed by Western blotting. Samples were either heat denatured and reduced with dithiothreitol before loading for detection of Nflag, M, and E or not heated and not reduced for analysis of S. Blots were exposed for 10 s for signal detection, except for E, for which the blots were exposed for 10 min. The highest levels of S, M, N, and E structural proteins were found in fractions 9 and 10 corresponding to 40% sucrose. S protein was detected with mouse polyclonal antibodies raised against purified S trimers. Arrows indicate bands that correspond to trimeric and monomeric forms of S. The molecular mass (in kilodaltons) and the migration of protein standards are shown on the right sides of the blots.

present in fractions 5 to 14 at proportional levels. E was detected in fractions 8 to 10, where M and N proteins were also enriched. Altogether, these results show that secreted viral structural proteins cosediment in sucrose gradient and therefore strongly suggest that viral proteins are associated into VLPs. Moreover, secretion of E-containing vesicles does not seem to be a major phenomenon in Vero E6 cells expressing E alone or in combination with other viral proteins in our system. Indeed, in all conditions, levels of E in cell medium were systematically low and only detected in fractions when coexpressed with M and N.

Altogether, these data establish for the first time that all three M, E, and N structural SARS-CoV proteins are important for the efficient production and release of SARS-CoV VLPs.

S is incorporated onto SARS-CoV M-E-N-containing VLPs. We then investigated whether the SARS-CoV S glycoprotein could be incorporated onto secreted M-E-N VLPs. S cDNA was codon optimized and subcloned in the pcDNA vector. Vero E6 cells were transfected with pIRES-M-E plus pcDNA-Nflag plus pcDNA-S. Protein expression was verified in cell lysates at 48 h posttransfection (data not shown). To monitor the association of S onto M-E-N VLPs, we performed sucrose fractionation on VLPs previously purified from culture medium (Fig. 2). All S, Nflag, M, and E proteins were cosedimented and enriched in fractions 9 and 10 corresponding to ~40% sucrose. It is notable that S was mainly detected in its native trimeric form in these fractions (540 kDa), although we also detected low levels of monomers (180 kDa) and dimers (360 kDa), which may have resulted from sample treatment and SDS-polyacrylamide gel electrophoresis conditions. Higher-molecular-weight proteins, detected with anti-S antibodies, were found in the lightest fractions 1 to 6. These forms could correspond to soluble, nonincorporated forms of S proteins that have formed aggregates. We have previously described the formation of S aggregates in preparations of purified SARS-CoV S trimers from mammalian cell lysates (31). This result confirms the association of all four SARS-CoV structural proteins into S-M-E-N VLPs that can be purified from the culture medium of transfected cells.

VLPs bud into a perinuclear compartment and are transported within vesicles to the plasma membrane. We next studied the subcellular localization of SARS-CoV VLPs by electron microscopy (Fig. 3). pIRES-M-E plus pcDNA-Nflag plus pcDNA-S cotransfected Vero E6 cells were fixed at 24 and 48 h posttransfection, and ultrathin sections were prepared for transmission electron microscopy (Fig. 3A to G). Large amounts of VLPs, with diameters ranging from 40 to 150 nm on the sections, were found within the cytoplasm of positive cells. Three main patterns of subcellular localization were observed. First, VLPs were found within perinuclear compartments, which had an appearance of groups of vacuoles (Fig. 3A, C, and D) or, alternatively but seldom observed, which presented morphological characteristics of the ER (Fig. 3B). Vacuoles were observed at both 24 and 48 h posttransfection with a diameter ranging from 300 nm to 1.5 μm on the sections. Very interestingly, we detected several events of VLP budding at vacuole membranes (Fig. 3D). Although VLPs accumulated therein, they were not highly compacted in this compartment. Moreover, VLPs appeared pleiomorphic and heterogeneous material was also observed (Fig. 3D). Tubular structures were seen within some VLP-containing vacuoles, mainly at 24 h posttransfection (data not shown). Second, VLPs were observed in vesicles scattered in the cytoplasm (Fig. 3A, B, C, and E). These vesicles had a diameter ranging from 200 nm to 1 μm on sections, and the VLPs were more compacted inside. They could be found near the perinuclear VLP-containing compartments up to the cortical area. VLPs contained in these vesicles looked more homogeneous in size and shape. Third, VLPs were occasionally found at the cell surface (Fig. 3A, F, and G). Although we could not observe obvious spikelike structures surrounding the VLP envelope, spikelike protuberances were occasionally detected (Fig. 3G). Moreover, binding of VLPs to the cell surface suggests the presence of spikes and receptor recognition. Some cells, in which very high amounts of VLPs were found, presented characteristics of apoptosis with fragmented nucleus and disrupted membranes (data not shown). The cytoplasm of these cells was filled up with VLPs, either free or within intracellular compartments. The morphology of released VLPs was investigated further by electron microscopy on negatively stained particles that were purified from the cell medium (Fig. 3F). Round particles with a diameter of 80 to 100 nm were readily observed. Again, we could not observe the typical corona of spikes around VLPs (21), but globular structures protruding from VLPs were detected, which likely corresponded to trimers of the spikes. Altogether, our data suggest that SARS-CoV VLPs bud in an intracellular compartment of Vero E6 cells and are efficiently transported within vesicles to the plasma membrane where they are released. The shapes and sizes of the secreted VLPs are in accordance with the morphological characteristics of the SARS-CoV, and therefore these VLPs should be a safe and appropriate model for studying the assembly and release of SARS-CoV virions.

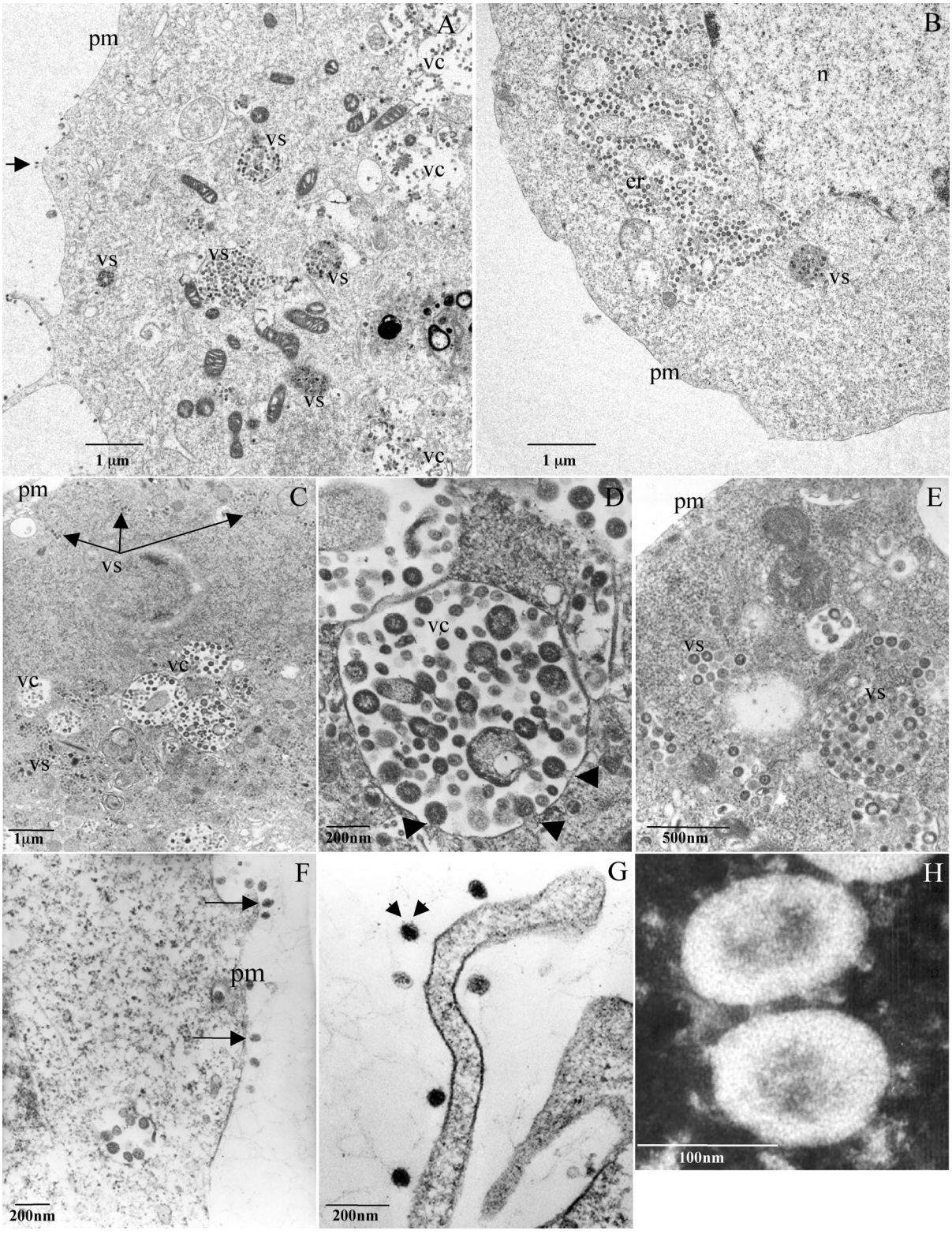

FIG. 3. Structural analysis and intracellular distribution of SARS-CoV VLPs. Vero E6 cells were cotransfected with pIRES-M-E, pcDNA-Nflag, and pcDNA-S. At 24 and 48 h posttransfection the cells were fixed, and ultrathin sections were analyzed by electron microscopy (A to G). (A) VLPs were found in intracellular vacuoles (vc) and in vesicles (vs) scattered in the cytosol and bound to the plasma membrane (pm). The arrow points to VLPs attached to the cell surface. (B) Large amount of VLPs within the lumen of the endoplasmic reticulum (er) and within a cytoplasmic vesicle. n, nucleus. (C) Presence of VLPs within vacuoles and vesicles. Arrows point to small VLPs-containing vesicles beneath the plasma membrane. (D) Magnification of a VLP-containing vacuole. Black arrows point to budding events. (E) Compacted VLP-containing vesicles were found beneath the plasma membrane. (F) VLPs bound to the surface of a producer cell. Two membrane-bound VLPs are indicated by arrows. (G) VLPs bound to a cell filopodia. Spikelike protuberances were visible on the VLP surface (arrows). (H) Electron microscopy images of negatively stained VLPs purified from cell medium at 48 h posttransfection. A scale bar is indicated for each picture. Panels A to D and panels F to G correspond to cells fixed at 48 h posttransfection. The image in panel E was taken from cells fixed at 24 h posttransfection. n, nucleus; er, ER; vc, vacuole; vs, vesicle; pm, plasma membrane.

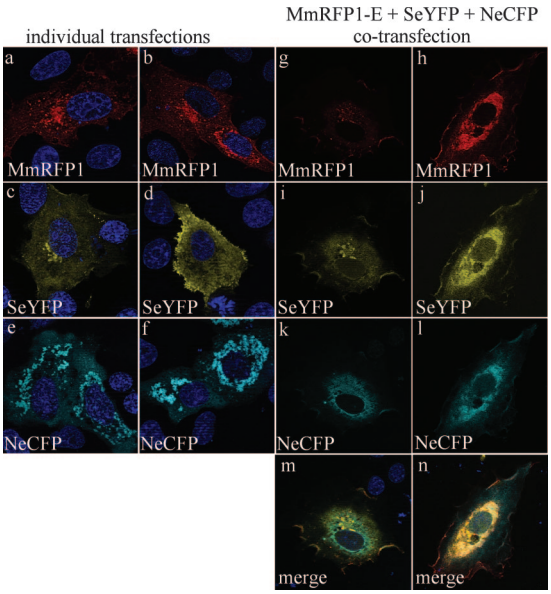

FIG. 4. Expression and subcellular distribution of viral structural proteins tagged with fluorescent proteins. Vero E6 cells grown on glass coverslips were either transfected with single plasmids (left panels) or cotransfected (right panels) with the three plasmids encoding the MmRFP1, E, SeYFP, and NeCFP proteins. At 24 h posttransfection, cells were processed for nuclear staining with DAPI dye, fixed, and analyzed under a fluorescence microscope equipped with an ApoTome device to acquire images of optical sections. a, b, g, and h, MmRFP1; c, d, i, and j, SeYFP; e, f, k, and l, NeCFP; m and n, merged images. For all conditions, two representative images are shown side by side.

Assembly and release of VLPs that incorporate fluorescently tagged structural viral proteins. In order to visualize in real time the assembly, trafficking, and release of SARS-CoV VLPs, we engineered plasmid constructs that allow expression of viral proteins in fusion with fluorescent proteins. The pIRES-MmRFP1-E, pcDNA-NeCFP, and pcDNA-SeYFP constructs were developed, and the expression of fusion viral proteins was analyzed in individually transfected or cotransfected cells by fluorescence microscopy (Fig. 4). We did not include any construct coding for a fluorescently tagged SARS-CoV E protein because it does not tolerate fluorescent protein tags (C. Chan et al., unpublished data). All chimeric viral proteins could be readily observed by fluorescence microscopy. In cells individually transfected with the pIRES-MmRFP1-E, the MmRFP1 fusion protein was mainly present in a perinuclear compartment, most likely the ERGIC/Golgi apparatus (Fig. 4a and b). We also found MmRFP1 within the cytoplasm and occasionally at the plasma membrane. As expected, the SeYFP protein was observed both in the ERGIC/Golgi apparatus and at the plasma membrane of individually transfected cells (Fig. 4c and d). These expression patterns are similar to what we observed previously for MeGFP and SeGFP fusion proteins at 15 h postinfection with Semliki Forest virus expression vectors (51). In most of the cells, individually expressed NeCFP protein formed bright cytosolic patches, suggesting aggregation of the protein in the cytosol in the absence of functional viral protein partners (Fig. 4e and f). This pattern may reflect large inclusions of nucleocapsids, which have been described to accumulate late in the infection of cells with HCoV and MHV-JHM and SARS-CoV (6, 17, 23) or may constitute a cytosolic reservoir of protein supposed to feed the viral budding system. Interestingly, when plasmids were cotransfected, all three MmRFP1, SeYFP, and NeCFP fluorescent proteins presented similar intracellular distributions, colocalizing in the cytoplasm and at the plasma membrane (Fig. 4g, i, k, and m and Fig. 4h, j, l, and n). When coexpressed with MmRFP1, E, and SeYFP, the subcellular distribution of the NeCFP protein was dramatically changed, and bright cytosolic patches were rarely found (Fig. 4e and f and Fig. 4k and l). Trafficking of NeCFP to the cell surface in cotransfected cells suggests that interactions with other viral proteins have occurred, leading to NeCFP translocation. Nevertheless, no VLPs were detected in medium from cotransfected cells (data not shown). Altogether, these results suggest that although MmRFP1, SeYFP, NeCFP, and E are likely to interact when coexpressed in Vero E6 cells, they are not released in the form of VLPs in cell medium.

We then reasoned that fluorescent VLPs could be produced by including only one plasmid coding for one of the fluorescently tagged viral protein per cotransfection. In these conditions, we investigated protein expression and release of VLPs by Vero E6 cells at 48 h posttransfection (Fig. 5A). As a positive control, we monitored VLP release from pIRES-M-E, pcDNA-Nflag, pcDNA-S transfected cells. As expected, S, Nflag, M, and E proteins were detected in both the cell lysate and the VLP preparation (Fig. 5A, lanes 2 and 7). Although the MmRFP1 fusion protein was readily observed by fluorescence microscopy, it could not be detected by Western blotting. Most likely, the rabbit polyclonal antibody directed against the M C-terminal domain cannot recognize its epitope when it is fused to the mRFP1 fluorescent tag. Although the E, Nflag and S proteins were detected on the cell lysate from pIRES-MmRFP1-E plus pcDNA-Nflag plus pcDNA-S transfected cells (Fig. 5A, lane 3), no protein corresponding to purified VLPs was found in the medium (Fig. 5A, lane 8). We concluded that fusion of the mRFP1 protein at the C-terminal end of M inhibits VLP production. On the contrary, both pIRES-M-E plus pcDNA-NeCFP plus pcDNA-S, as well as pIRES-M-E plus pcDNA-Nflag plus pcDNA-SeYFP transfected cells were able to release VLPs in cell medium, as indicated by the presence of viral proteins (Fig. 5A, lanes 9 and 10). Under these conditions, the NeCFP protein was detected by a mouse monoclonal antibody directed against N (56) and migrated to an apparent molecular size of 70 kDa.

To confirm that NeCFP or SeYFP viral proteins are correctly incorporated into VLPs, we analyzed purified VLPs by fractionation on a 20 to 60% sucrose gradient (Fig. 5B). Both NeCFP and SeYFP cosedimented with other viral proteins, indicating that they were incorporated in purified VLPs (Fig. 5B, upper and lower panels, respectively). M-E-NeCFP-S VLPs were concentrated in fractions 10 and 11. The E protein was not detected, most likely because M-E-NeCFP-S VLPs were less abundant in culture medium than M-E-Nflag-S VLPs for which the E levels were already low. M-E-Nflag-SeYFP VLPs were more efficiently produced and concentrated in fractions 9 and 10, although high levels were also found in fractions 6, 7, and 8. Considering the high levels of M and Nflag detected in these fractions, incorporation of SeYFP seems less efficient than S (cf. Fig. 2 with Fig. 5B, lower panel). Altogether, our

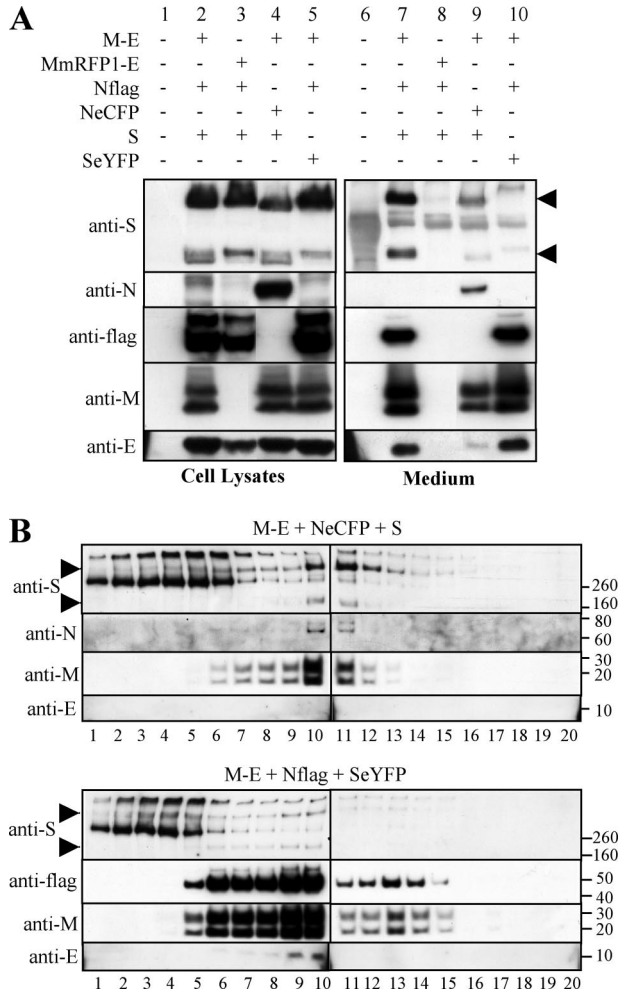

FIG. 5. Production of fluorescent VLPs by transfected Vero E6 cells. (A) Determination of optimal plasmid combinations for production of SARS-CoV fluorescent VLPs. Viral proteins from cell lysates (left panel) and sedimented VLPs from medium (right panel) were analyzed by Western blotting. VLPs could be produced when either N or S (lanes 9 and 10) but not M (lane 8) were tagged with fluorescent proteins. (B) Production of fluorescent VLPs and efficiency of incorporation of NeCFP and SeYFP fusion proteins into VLPs. Cells were cotransfected with the specified plasmid combinations (corresponding to lanes 9 and 10 of panel A), and purified VLPs from medium were analyzed by using a sucrose gradient. Tagging S (lower blot) resulted in a greater yield of VLP production compared to tagged N (upper blot). However, the eYFP tag greatly reduced S incorporation into VLPs (lower blot). Arrowheads indicate spike trimers and monomers.

results demonstrate that fluorescent VLPs can be readily produced in Vero E6 transfected cells by incorporating either a tagged N or S fusion protein.

Visualization of M-E-NeC/GFP-S VLP production and transport in living Vero E6 cells. We then investigated the formation and transport of fluorescent SARS-CoV VLPs in living transfected cells by fluorescence microscopy. Knowing that S is expressed all along the secretory pathway in both singly transfected and cotransfected cells, we reasoned that N would be a better marker for monitoring of SARS-CoV VLP assembly. Furthermore, having demonstrated that M, E, and N are the crucial factors for the assembly and egress of SARS-CoV VLPs and anticipating that S-bearing VLPs could be internalized back into producer cells by ACE-2-driven endocytosis, we decided to omit S. Therefore, the pcDNA-NeCFP plasmid was either transfected alone or cotransfected with pIRES-M-E. Vero E6 cells were analyzed at 24 h posttransfection. In most pcDNA-NeCFP transfected cells, eCFP signals were very bright and concentrated in large aggregates in the cytosol at the periphery of the nucleus (Fig.6Aa). Inversely and very interestingly, a different pattern was observed in most of cells cotransfected with pIRES-M-E and pcDNA-NeCFP. In these cells, eCFP fluorescence was more diffuse in the cell cytosol: medium-size bright vesicles were concentrated in close proximity to the nucleus, smaller and dimmer vesicles were scattered in the cytoplasm, and occasionally bright dots were enriched at the cell cortical area (Fig.6Ab). A few bright dots were also found outside the cells in the surrounding medium. This difference in NeCFP distribution pattern suggests that NeCFP assembles with coexpressed M and E viral proteins to form VLPs and traffics from the perinuclear assembly compartment to the cell surface, where fluorescent VLPs are released into the medium.

We then further analyzed the trafficking dynamics of a fluorescently tagged N protein, coexpressed with M and E envelope proteins in living Vero E6 cells. Images were acquired by using a spinning disc confocal microscope coupled to a charge-coupled device camera suitable for high-speed and high-resolution imaging. In these experiments we replaced the NeCFP by a NeGFP fusion protein, which is excitable by the argon laser the microscope was equipped with. We could consistently identify three types of NeGFP containing vesicles, where fluorescent signal intensities, sizes, and movements differ (Fig. 6B; corresponding videos are provided in the supplemental material). First, the largest and brightest vesicles were found close to the nucleus and were static. Second, smaller and dimmer vesicles were trafficking actively, most of the time in a multidirectional way, making transient interactions with other vesicles. Occasionally, these vesicles moved in rapid, unidirectional way and for longer distances, most likely along microtubules. Third, some cells presented an accumulation of bright dots at the cortical area, which may correspond to smaller secretory vesicles and released VLPs. A few bright dots were found outside cells, which probably correspond to fluorescent VLPs that have been released from producer cells. These results illustrate that fusion of a fluorescent tag to the C-terminal end of the nucleocapsid viral protein makes monitoring of SARS-CoV VLPs' egress possible.

We then investigated the effect of BFA, a fungal metabolite that has multiple effects upon the organelles of the secretory pathway, including inhibition of trafficking from ER to the Golgi apparatus, fusion of the cisternae of the Golgi with the ER, and fusion of the trans-Golgi network with endosomes (59). BFA has been used in previous studies for analysis of viral protein transport and virus assembly (10, 49). Time-lapse images of living Vero E6 cells transfected with M-E plus NeGFP were acquired at 24 h posttransfection (Fig. 6C; for a video, see the supplemental material). In a first time, cells were either not treated (Fig.6Ca) or treated with 6 μg of BFA/ml for 4 h (Fig.6Cd) or overnight (Fig.6Cg). After several minutes of acquisition in these conditions, medium was changed to either BFA-containing medium (Fig. 6Cb and c) or normal medium

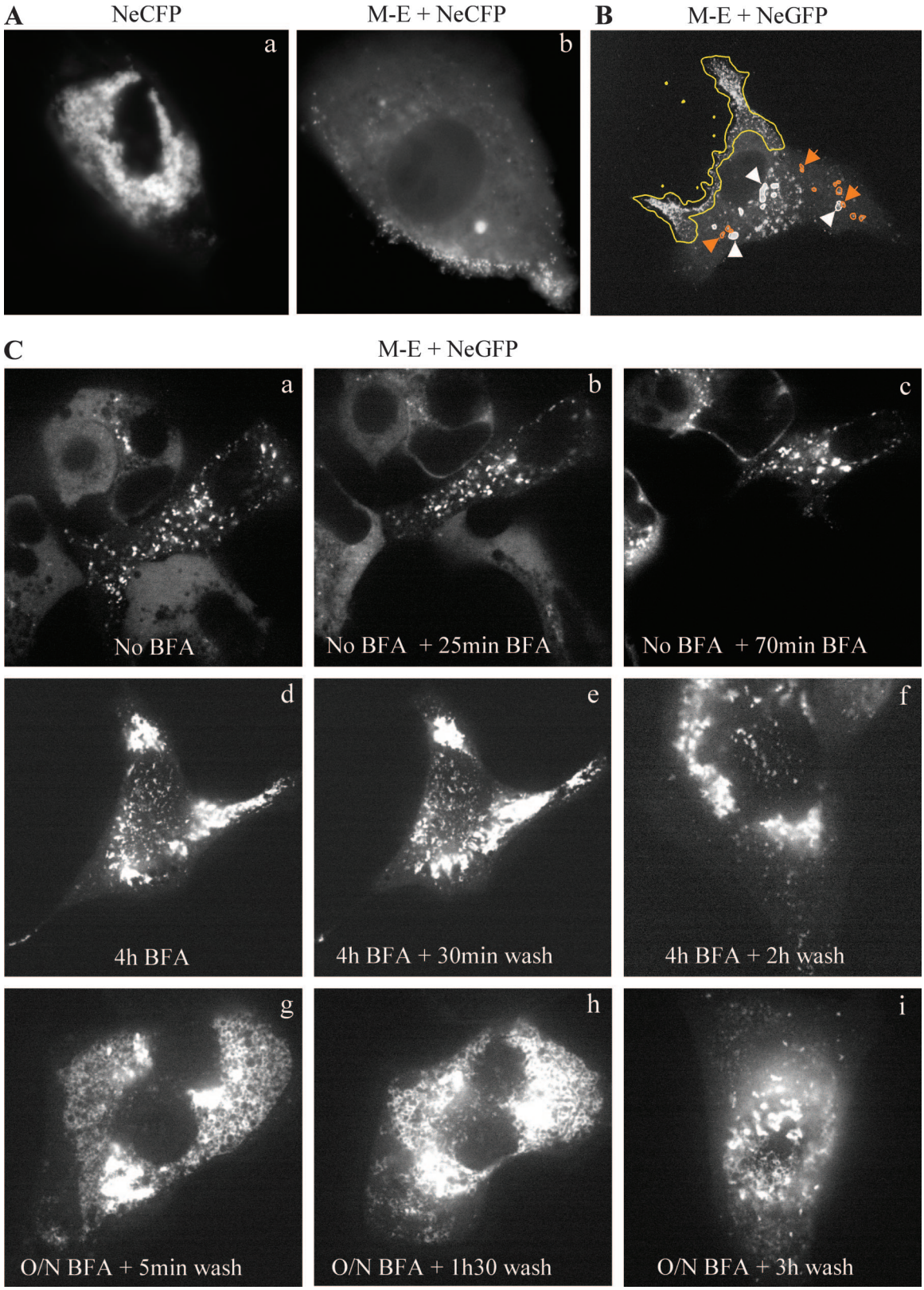

FIG. 6. Tracking of fluorescent SARS-CoV VLPs in living cells. (A) Wide-field fluorescence microscopy images showing the accumulation of fluorescent VLPs at the plasma membrane of pIRES-M-E plus pcDNA-NeCFP cotransfected cells (panel b), whereas a strong perinuclear staining was observed in Vero E6 cells expressing NeCFP alone (panel a). (B) Confocal microscopy of living cells expressing M-E-NeGFP VLPs. Four categories of fluorescent signals were observed: a bright and static large perinuclear compartment (white encircling lines), smaller and dimmer actively trafficking vesicles (orange encircling lines), bright dots accumulating at the cell cortex (yellow encircling lines), and dots in the medium

(Fig. 6Ce and f and Fig. 6Ch and i), respectively. New sequences of images were acquired, and the fluorescence redistribution was analyzed. Upon BFA treatment we observed fusion of scattered fluorescent vesicles into large cytosolic fluorescent clusters accumulating at the center of the cell and diminution of puncta (Fig. 6Ca, b and c and see also the supplemental material). After treatment of cells for 4 h with BFA, most of the fluorescence was present in large bright patches surrounding the nucleus (Fig. 6Cd). Vesicles could still be observed in the cytosol, although they were less numerous than in nontreated cells. After a BFA wash step, we could not observe any obvious reversibility of the massive redistribution of fluorescence (compare Fig. 6Cd and e and Fig. 6Cf). After overnight incubation with BFA, fluorescence was associated with large cytosolic clusters and ER (Fig. 6Cg), and no drastic change was observed after the BFA wash and recovery for 1 h 30 min (Fig. 6Ch), although membrane dynamics seem to increase at the edge on the reticular compartment, where tubules were elongated (Fig. 6Ch; see also the supplemental material). A 3-h recovery period after overnight BFA treatment partially restored trafficking of fluorescent vesicles in transfected cells (Fig. 6Ci). The recovery process after BFA treatment was slow, and the dynamics could not be followed for several hours, because repetitive exposure to laser induced apoptosis. Altogether, our results suggest (i) that BFA induces reorganization of NeGFP-associated compartments and alters vesicle formation and transport and (ii) that a period of several hours of recovery after a BFA washing step is necessary in order to restore the dynamics of the NeGFP-associated compartment and vesicle trafficking. Further studies are needed in order to clarify what subcellular compartment VLPs are associated with and delineate the dynamics of egress in association with cellular structures.

DISCUSSION

The minimal molecular requirement for efficient assembly and egress of SARS-CoV virions is still controversial. We describe here the development of a plasmid-based transfection method for the efficient production and release of SARS-CoV VLPs in permissive Vero E6 green monkey kidney epithelial cells. In contrast to reports on other coronaviruses, we demonstrate that all three M, E, and N SARS-CoV structural proteins are required for the efficient assembly and release of VLPs by transfected cells. When the S viral envelope glycoprotein is coexpressed with M, N, and E, trimers of S are incorporated into VLPs. Of particular interest is the finding that incorporation of a fluorescently tagged N protein into VLPs allows visualization of transport of de novo formed particles in producer cells. Fluorescent VLPs constitute a new powerful model for studying the mechanisms of SARS-CoV egress in living cells and the specific roles of cellular machineries by fluorescence imaging techniques.

Other research groups have described the formation of SARS-CoV VLPs in either insect (26, 44, 50) or mammalian (27–29) cells, using various expression systems. Y. Huang et al. were the first to report the generation of SARS-CoV VLPs in human 293 renal epithelial cells (29). Human codon optimized genes encoding for M, E, N, and S proteins were subcloned into mammalian expression vector, and VLP formation was monitored by transmission electron microscopy on transfected cells at 63 h posttransfection. These authors show that, in their experimental conditions, M and N are necessary and sufficient for the formation of intracellular VLPs, independently of E and S, but the secretion of VLPs was not efficient. Moreover, they described S as being an important viral factor for the maturation and egress of VLPs from cells, but the release of M-N-S VLPs in culture medium was still inefficient. In contrast, in our system we detected sedimentable M and N proteins in culture medium from M- plus N-expressing cells, suggesting that M-N VLPs can form and be secreted (Fig. 1). Furthermore, the coexpression of E greatly boosted the levels of VLPs detected in the culture medium (Fig. 1), and the addition of S did not influence the rate of VLP production (Fig. 2 and data not shown). In contrast, Hsieh et al. (27) have shown that coexpressed E and M proteins are released 4 days posttransfection in culture medium of Vero E6 cells in the absence of S and N proteins. In that study, Vero E6 cells, previously infected with a recombinant vaccinia virus harboring the T7 polymerase gene, were cotransfected with plasmids encoding MycHis or V5His-tagged S, M, E, and N structural proteins. Nevertheless, sedimentable E and M proteins were also found in the culture medium even when they were individually expressed, and very high amounts of E were found in VLP preparations in comparison to other viral proteins, suggesting the formation of E-containing vesicles. Others have shown that MHV and infectious bronchitis virus E protein expressed alone results in the assembly of E-protein-containing vesicles, with a density similar to that of VLPs (7, 47). We also found sedimentable SARS-CoV E proteins in culture medium from individually pcDNA-E transfected cells, suggesting the secretion of E vesicles, but we could not detect them in any fraction after sucrose gradient fractionation, suggesting a low production rate (Fig. 1). We could also detect M-E VLPs at 48 h posttransfection by coexpressing both E and M proteins, albeit at very low levels (Fig. 1). In our study, we took advantage of the pIRES bicistronic vector to ensure the concomitant expression of E and M and to maintain a low expression level for E. We show that the use of this vector system, in combination with the expression of N, ensures slightly better levels of M-E-N VLPs in the medium and great incorporation of E (Fig. 1B). Higher levels of E were expressed when an individual

surrounding transfected cells (yellow dots). Videos are available in the supplemental material. (C) Treatment of transfected cells with BFA alters the trafficking of fluorescent vesicles. Vero E6 cells were transfected with pIRES-M-E plus pcDNA-NeGFP plasmids. Cells were either not treated (panel a) or treated with 6 μg of BFA/ml for either 4 h (panel d) or overnight (panel g). BFA was then added to untreated cells, and time-lapse acquisitions were performed. Panels b and c show the same cells as in panel a but after 25- and 70-min incubations with the drug. Alternatively, BFA was washed out and recovery after BFA treatment was analyzed (panels e and f and panels h and i). Panels a, b, and c, panels d and e, and panels g and h show the same cells at different time points. Videos illustrating panels b, f, h, and i are provided in the supplemental material.

pcDNA-E vector was used for E expression and resulted in increased E/M and E/N ratios in the cell medium (Fig. 1B). We could not conclude whether this was due to a higher level of E incorporation into VLPs or to a simultaneous release of E-containing vesicles and VLPs. Analysis of viral protein in cell medium by sucrose gradient fractionation revealed that E was only released at significant levels when coexpressed with M and N proteins, with which it cosediments (Fig. 1Cb, c, and e). We have observed efficient M-E-N-S VLP formation and release in 293T, HeLa, and Huh-7 human cell lines (data not shown). Consistently, the formation and release of M-E-N-S VLPs from 293T cells has been shown in another study reported by C. Huang et al., in which the authors used a pCAGGS mammalian expression plasmid-based transfection system (28). Lokugamage and coworkers were able to generate approximately 1.3 μg of SARS-CoV VLPs from 2×10^7 293T cells (42). Recently, we have measured the quantity of S incorporated into the envelopes of M-E-N-S VLPs purified from the VLP-containing sucrose fractions in our system. Approximately 1 and 28 μg of S were present in VLP preparations from 10^7 VeroE6 and 293T cells, respectively (data not shown).

We also investigated the formation and secretion of SARS-CoV VLPs in transfected cells by transmission electron microscopy and negative staining of purified secreted particles (Fig. 3). We were able to identify budding events in cytoplasmic perinuclear compartments. VLP-containing vesicles were scattered within the cytoplasm and found beneath the plasma membrane. Occasionally, secreted VLPs were bound to the cell surface. The VLP-associated compartments that we observed in transfected Vero E6 cells share significant similarities with the virion-containing compartments described in SARS-CoV-infected Vero E6 cells at 3 to 5 days postinfection (23). VLPs were readily detected in sedimented fractions from culture medium by negative staining and electron microscopy (Fig. 3H). Globular structures protruding from the VLP envelope, and which should correspond to spike peplomers, were occasionally detected, but we could not identify any particle displaying a typical corona-like structure which is the signature of the optimal incorporation of spike trimers on the virion envelope.

Interestingly, we found that a C-terminal Flag or eYFP tag affects the levels of S trimers incorporation into VLPs (data not shown or Fig. 5, respectively). However, Sflag and SeYFP proteins could still be incorporated into VLPs, and tags can be used as markers. Similar results had been obtained for MHV, where the S sequence had been extended by fusion with a GFP fluorescent protein (3). These data can be explained by several factors: the 30-kDa fluorescent protein may cause geometrical constraints; M-S interactions, which are important for S incorporation may be affected by the tag; and S retention to the site of viral assembly may be disturbed (43, 48). We also tried to produce VLPs containing the mRFP1 fluorescent protein fused to the C-terminal end of M (Fig. 4 and 5A). Although MmRFP1 was expressed in transfected cells, the production of VLPs was abrogated. The M endodomain is crucial for M-N, M-E, and M-S interactions and VLP formation (8, 13, 15, 19), and its fusion to a fluorescent protein tag may affect its structure and/or availability for interaction with other partners. This hypothesis is reinforced by the complete loss of recognition of the chimeric MmRFP1 by a rabbit serum raised against a C-terminal peptide of M (Fig. 5A, left panel).

Lastly, a fusion NeCFP protein could be expressed and assemble into VLPs with M, E, and S, although the levels of VLPs detected in culture medium were significantly reduced (Fig. 5). Interestingly, whereas individually expressed NeCFP or NeGFP were found in the cell cytosol, often accumulating in the perinuclear area, the tagged N protein had a tendency to display a vesicular distribution pattern when coexpressed with M and E (Fig. 6). We analyzed both the distribution and the trafficking of the NeGFP protein in transfected live cells by confocal microscopy (Fig. 6B). When cells were cotransfected with pIRES-M-E and pcDNA-NeGFP, the NeGFP proteins were often found in a static compartment near the nucleus, in trafficking vesicles scattered in the cytosol and moving actively, making transient interactions with other vesicles, and as small dots scattered in the cortical area beneath the plasma membrane, often enriched in cell projections. Fluorescent dots were also detected in the cell medium surrounding living cells. A subcellular distribution of NeGFP is consistent with our transmission electron microscopy data. Most likely, the perinuclear static compartments and trafficking vesicles identified by fluorescence microscopy correspond to perinuclear vacuoles, membranes where VLP budding events were observed, and to VLP-containing vesicles found by electron microscopy, respectively. The fluorescent dots observed in the cell cortical area may correspond to smaller secretory vesicles containing fewer VLPs—vesicles containing only one VLP were found by electron microscopy—and/or to released VLPs, which are bound to the cell surface. Interestingly, the transport of fluorescent vesicles was affected by the drug BFA, which is well known to affect membrane transport in the secretory pathway (39, 59). BFA treatment induced backward trafficking of fluorescent vesicles and fusion into bright perinuclear clusters (Fig. 6Ca, b, and c). Long-lasting BFA treatment resulted in the suppression of vesicle trafficking, no fluorescent puncta were found at plasma membrane (Fig.6Cg), and recovery of vesicle trafficking was restored after several hours in normal medium (Fig.6Ci).

Altogether, our data demonstrate that M, E, and N structural proteins are key molecules in the assembly and egress of the SARS-CoV. Production and analysis of fluorescent M-E-NeGFP SARS-CoV VLPs in living cells allowed us to identify three subcellular structures with different velocity characteristics along the secretory pathway. Molecular and cellular determinants of SARS-CoV assembly and egress will be investigated further using advanced fluorescence microscopy techniques.

ACKNOWLEDGMENTS

We thank K. H. Chan (Department of Microbiology, University of Hong Kong) for the gift of the mouse monoclonal antibody against the SARS-CoV N protein, V. Lorin (Institut Pasteur) for preparation and analysis of the anti-E rabbit serum, and Roger Y. Tsien (University of California, San Diego) for providing the plasmid coding for the mRFP1 protein. We especially thank the Electron Microscope Unit of the University of Hong Kong, Li Ka Shing Faculty of Medicine, and Marie-Christine Prevost and Martin Sachse (Plate-Forme de Microscopie Electronique, Institut Pasteur) for expert advice on the electron microscopy experiments; Iris Ng (Department of Microbiology, University of Hong Kong) for technical support for electron microscopy experiments; and Tony Chan (Department of Anatomy, Li Ka Shing Faculty of Medicine Core Imaging Facility, University of Hong Kong) for technical support during the live cell imaging experiments.

K.T.T. is a Ph.D. student supported by the University of Hong Kong. This study was supported by the French Ministry of Health (through the RESPARI Program of the International Network of Institut Pasteur), the French Chancery of Paris Universities, and the EU-6th Framework Program (EPISARS).

REFERENCES

1. **Baudoux, P., C. Carrat, L. Besnardeau, B. Charley, and H. Laude.** 1998. Coronavirus pseudoparticles formed with recombinant M and E proteins induce alpha interferon synthesis by leukocytes. J. Virol. **72:**8636–8643.
2. **Bos, E. C., W. Luytjes, H. V. van der Meulen, H. K. Koerten, and W. J. Spaan.** 1996. The production of recombinant infectious DI-particles of a murine coronavirus in the absence of helper virus. Virology **218:**52–60.
3. **Bosch, B. J., C. A. de Haan, and P. J. Rottier.** 2004. Coronavirus spike glycoprotein, extended at the carboxy terminus with green fluorescent protein, is assembly competent. J. Virol. **78:**7369–7378.
4. **Bosch, B. J., C. A. de Haan, S. L. Smits, and P. J. Rottier.** 2005. Spike protein assembly into the coronavirion: exploring the limits of its sequence requirements. Virology **334:**306–318.
5. **Campbell, R. E., O. Tour, A. E. Palmer, P. A. Steinbach, G. S. Baird, D. A. Zacharias, and R. Y. Tsien.** 2002. A monomeric red fluorescent protein. Proc. Natl. Acad. Sci. USA **99:**7877–7882.
6. **Caul, E. O., and S. I. Egglestone.** 1977. Further studies on human enteric coronaviruses. Arch. Virol. **54:**107–117.
7. **Corse, E., and C. E. Machamer.** 2000. Infectious bronchitis virus E protein is targeted to the Golgi complex and directs release of virus-like particles. J. Virol. **74:**4319–4326.
8. **Corse, E., and C. E. Machamer.** 2003. The cytoplasmic tails of infectious bronchitis virus E and M proteins mediate their interaction. Virology **312:**25–34.
9. **Curtis, K. M., B. Yount, and R. S. Baric.** 2002. Heterologous gene expression from transmissible gastroenteritis virus replicon particles. J. Virol. **76:**1422–1434.
10. **Dasgupta, A., and D. W. Wilson.** 2001. Evaluation of the primary effect of brefeldin A treatment upon herpes simplex virus assembly. J. Gen. Virol. **82:**1561–1567.
11. **Decaro, N., V. Mari, C. Desario, M. Campolo, G. Elia, V. Martella, G. Greco, F. Cirone, M. L. Colaianni, P. Cordioli, and C. Buonavoglia.** 2008. Severe outbreak of bovine coronavirus infection in dairy cattle during the warmer season. Vet. Microbiol. **126:**30–39.
12. **DeDiego, M. L., E. Alvarez, F. Almazan, M. T. Rejas, E. Lamirande, A. Roberts, W. J. Shieh, S. R. Zaki, K. Subbarao, and L. Enjuanes.** 2007. A severe acute respiratory syndrome coronavirus that lacks the E gene is attenuated in vitro and in vivo. J. Virol. **81:**1701–1713.
13. **de Haan, C. A., L. Kuo, P. S. Masters, H. Vennema, and P. J. Rottier.** 1998. Coronavirus particle assembly: primary structure requirements of the membrane protein. J. Virol. **72:**6838–6850.
14. **de Haan, C. A., and P. J. Rottier.** 2005. Molecular interactions in the assembly of coronaviruses. Adv. Virus Res. **64:**165–230.
15. **de Haan, C. A., M. Smeets, F. Vernooij, H. Vennema, and P. J. Rottier.** 1999. Mapping of the coronavirus membrane protein domains involved in interaction with the spike protein. J. Virol. **73:**7441–7452.
16. **de Haan, C. A., H. Vennema, and P. J. Rottier.** 2000. Assembly of the coronavirus envelope: homotypic interactions between the M proteins. J. Virol. **74:**4967–4978.
17. **Dubois-Dalcq, M. E., E. W. Doller, M. V. Haspel, and K. V. Holmes.** 1982. Cell tropism and expression of mouse hepatitis viruses (MHV) in mouse spinal cord cultures. Virology **119:**317–331.
18. **Erles, K., C. Toomey, H. W. Brooks, and J. Brownlie.** 2003. Detection of a group 2 coronavirus in dogs with canine infectious respiratory disease. Virology **310:**216–223.
19. **Escors, D., J. Ortego, H. Laude, and L. Enjuanes.** 2001. The membrane M protein carboxy terminus binds to transmissible gastroenteritis coronavirus core and contributes to core stability. J. Virol. **75:**1312–1324.
20. **Fischer, F., C. F. Stegen, P. S. Masters, and W. A. Samsonoff.** 1998. Analysis of constructed E gene mutants of mouse hepatitis virus confirms a pivotal role for E protein in coronavirus assembly. J. Virol. **72:**7885–7894.
21. **Fouchier, R. A., T. Kuiken, M. Schutten, G. van Amerongen, G. J. van Doornum, B. G. van den Hoogen, M. Peiris, W. Lim, K. Stohr, and A. D. Osterhaus.** 2003. Aetiology: Koch's postulates fulfilled for SARS virus. Nature **423:**240.
22. **Godet, M., R. L'Haridon, J. F. Vautherot, and H. Laude.** 1992. TGEV corona virus ORF4 encodes a membrane protein that is incorporated into virions. Virology **188:**666–675.
23. **Goldsmith, C. S., K. M. Tatti, T. G. Ksiazek, P. E. Rollin, J. A. Comer, W. W. Lee, P. A. Rota, B. Bankamp, W. J. Bellini, and S. R. Zaki.** 2004. Ultrastructural characterization of SARS coronavirus. Emerg. Infect. Dis. **10:**320–326.
24. **He, R., F. Dobie, M. Ballantine, A. Leeson, Y. Li, N. Bastien, T. Cutts, A. Andonov, J. Cao, T. F. Booth, F. A. Plummer, S. Tyler, L. Baker, and X. Li.** 2004. Analysis of multimerization of the SARS coronavirus nucleocapsid protein. Biochem. Biophys. Res. Commun. **316:**476–483.
25. **He, R., A. Leeson, M. Ballantine, A. Andonov, L. Baker, F. Dobie, Y. Li, N. Bastien, H. Feldmann, U. Strocher, S. Theriault, T. Cutts, J. Cao, T. F. Booth, F. A. Plummer, S. Tyler, and X. Li.** 2004. Characterization of protein-protein interactions between the nucleocapsid protein and membrane protein of the SARS coronavirus. Virus Res. **105:**121–125.
26. **Ho, Y., P. H. Lin, C. Y. Liu, S. P. Lee, and Y. C. Chao.** 2004. Assembly of human severe acute respiratory syndrome coronavirus-like particles. Biochem. Biophys. Res. Commun. **318:**833–838.
27. **Hsieh, P. K., S. C. Chang, C. C. Huang, T. T. Lee, C. W. Hsiao, Y. H. Kou, I. Y. Chen, C. K. Chang, T. H. Huang, and M. F. Chang.** 2005. Assembly of severe acute respiratory syndrome coronavirus RNA packaging signal into virus-like particles is nucleocapsid dependent. J. Virol. **79:**13848–13855.
28. **Huang, C., N. Ito, C. T. Tseng, and S. Makino.** 2006. Severe acute respiratory syndrome coronavirus 7a accessory protein is a viral structural protein. J. Virol. **80:**7287–7294.
29. **Huang, Y., Z. Y. Yang, W. P. Kong, and G. J. Nabel.** 2004. Generation of synthetic severe acute respiratory syndrome coronavirus pseudoparticles: implications for assembly and vaccine production. J. Virol. **78:**12557–12565.
30. **Hurst, K. R., L. Kuo, C. A. Koetzner, R. Ye, B. Hsue, and P. S. Masters.** 2005. A major determinant for membrane protein interaction localizes to the carboxy-terminal domain of the mouse coronavirus nucleocapsid protein. J. Virol. **79:**13285–13297.
31. **Kam, Y. W., F. Kien, A. Roberts, Y. C. Cheung, E. W. Lamirande, L. Vogel, S. L. Chu, J. Tse, J. Guarner, S. Zaki, K. Subbarao, M. Peiris, B. Nal, and R. Altmeyer.** 2007. Antibodies against trimeric S glycoprotein protect hamsters against SARS-CoV challenge despite their capacity to mediate FcγRII-dependent entry into B cells in vitro. Vaccine **25:**729–740.
32. **Klumperman, J., J. K. Locker, A. Meijer, M. C. Horzinek, H. J. Geuze, and P. J. Rottier.** 1994. Coronavirus M proteins accumulate in the Golgi complex beyond the site of virion budding. J. Virol. **68:**6523–6534.
33. **Krijnse-Locker, J., M. Ericsson, P. J. Rottier, and G. Griffiths.** 1994. Characterization of the budding compartment of mouse hepatitis virus: evidence that transport from the RER to the Golgi complex requires only one vesicular transport step. J. Cell Biol. **124:**55–70.
34. **Ksiazek, T. G., D. Erdman, C. S. Goldsmith, S. R. Zaki, T. Peret, S. Emery, S. Tong, C. Urbani, J. A. Comer, W. Lim, P. E. Rollin, S. F. Dowell, A. E. Ling, C. D. Humphrey, W. J. Shieh, J. Guarner, C. D. Paddock, P. Rota, B. Fields, J. DeRisi, J. Y. Yang, N. Cox, J. M. Hughes, J. W. LeDuc, W. J. Bellini, and L. J. Anderson.** 2003. A novel coronavirus associated with severe acute respiratory syndrome. N. Engl. J. Med. **348:**1953–1966.
35. **Kuo, L., K. R. Hurst, and P. S. Masters.** 2007. Exceptional flexibility in the sequence requirements for coronavirus small envelope protein function. J. Virol. **81:**2249–2262.
36. **Kuo, L., and P. S. Masters.** 2002. Genetic evidence for a structural interaction between the carboxy termini of the membrane and nucleocapsid proteins of mouse hepatitis virus. J. Virol. **76:**4987–4999.
37. **Kuo, L., and P. S. Masters.** 2003. The small envelope protein E is not essential for murine coronavirus replication. J. Virol. **77:**4597–4608.
38. **Lim, K. P., and D. X. Liu.** 2001. The missing link in coronavirus assembly. Retention of the avian coronavirus infectious bronchitis virus envelope protein in the pre-Golgi compartments and physical interaction between the envelope and membrane proteins. J. Biol. Chem. **276:**17515–17523.
39. **Lippincott-Schwartz, J., L. C. Yuan, J. S. Bonifacino, and R. D. Klausner.** 1989. Rapid redistribution of Golgi proteins into the ER in cells treated with brefeldin A: evidence for membrane cycling from Golgi to ER. Cell **56:**801–813.
40. **Liu, D. X., and S. C. Inglis.** 1991. Association of the infectious bronchitis virus 3c protein with the virion envelope. Virology **185:**911–917.
41. **Locker, J. K., D. J. Opstelten, M. Ericsson, M. C. Horzinek, and P. J. Rottier.** 1995. Oligomerization of a trans-Golgi/trans-Golgi network retained protein occurs in the Golgi complex and may be part of its retention. J. Biol. Chem. **270:**8815–8821.
42. **Lokugamage, K. G., N. Yoshikawa-Iwata, N. Ito, D. M. Watts, P. R. Wyde, N. Wang, P. Newman, C. T. Kent Tseng, C. J. Peters, and S. Makino.** 2008. Chimeric coronavirus-like particles carrying severe acute respiratory syndrome coronavirus (SCoV) S protein protect mice against challenge with SCoV. Vaccine **26:**797–808.
43. **Lontok, E., E. Corse, and C. E. Machamer.** 2004. Intracellular targeting signals contribute to localization of coronavirus spike proteins near the virus assembly site. J. Virol. **78:**5913–5922.
44. **Lu, X., Y. Chen, B. Bai, H. Hu, L. Tao, J. Yang, J. Chen, Z. Chen, Z. Hu, and H. Wang.** 2007. Immune responses against severe acute respiratory syndrome coronavirus induced by virus-like particles in mice. Immunology **122:**496–502.
45. **Luo, H., D. Wu, C. Shen, K. Chen, X. Shen, and H. Jiang.** 2006. Severe acute respiratory syndrome coronavirus membrane protein interacts with nucleocapsid protein mostly through their carboxyl termini by electrostatic attraction. Int. J. Biochem. Cell. Biol. **38:**589–599.
46. **Madan, V., J. Garcia Mde, M. A. Sanz, and L. Carrasco.** 2005. Viroporin activity of murine hepatitis virus E protein. FEBS Lett. **579:**3607–3612.
47. **Maeda, J., A. Maeda, and S. Makino.** 1999. Release of coronavirus E protein

in membrane vesicles from virus-infected cells and E protein-expressing cells. Virology **263:**265–272.
48. **McBride, C. E., J. Li, and C. E. Machamer.** 2007. The cytoplasmic tail of the severe acute respiratory syndrome coronavirus spike protein contains a novel endoplasmic reticulum retrieval signal that binds COPI and promotes interaction with membrane protein. J. Virol. **81:**2418–2428.
49. **Mirazimi, A., C. H. von Bonsdorff, and L. Svensson.** 1996. Effect of brefeldin A on rotavirus assembly and oligosaccharide processing. Virology **217:**554–563.
50. **Mortola, E., and P. Roy.** 2004. Efficient assembly and release of SARS coronavirus-like particles by a heterologous expression system. FEBS Lett. **576:**174–178.
51. **Nal, B., C. Chan, F. Kien, L. Siu, J. Tse, K. Chu, J. Kam, I. Staropoli, B. Crescenzo-Chaigne, N. Escriou, S. van der Werf, K. Y. Yuen, and R. Altmeyer.** 2005. Differential maturation and subcellular localization of severe acute respiratory syndrome coronavirus surface proteins S, M, and E. J. Gen. Virol. **86:**1423–1434.
52. **Narayanan, K., K. H. Kim, and S. Makino.** 2003. Characterization of N protein self-association in coronavirus ribonucleoprotein complexes. Virus Res. **98:**131–140.
53. **Narayanan, K., A. Maeda, J. Maeda, and S. Makino.** 2000. Characterization of the coronavirus M protein and nucleocapsid interaction in infected cells. J. Virol. **74:**8127–8134.
54. **Narayanan, K., and S. Makino.** 2001. Characterization of nucleocapsid-M protein interaction in murine coronavirus. Adv. Exp. Med. Biol. **494:**577–582.
55. **Nguyen, V. P., and B. G. Hogue.** 1997. Protein interactions during coronavirus assembly. J. Virol. **71:**9278–9284.
56. **Nicholls, J. M., J. Butany, L. L. Poon, K. H. Chan, S. L. Beh, S. Poutanen, J. S. Peiris, and M. Wong.** 2006. Time course and cellular localization of SARS-CoV nucleoprotein and RNA in lungs from fatal cases of SARS. PLoS Med. **3:**e27.
57. **Ortego, J., D. Escors, H. Laude, and L. Enjuanes.** 2002. Generation of a replication-competent, propagation-deficient virus vector based on the transmissible gastroenteritis coronavirus genome. J. Virol. **76:**11518–11529.
58. **Peiris, J. S., S. T. Lai, L. L. Poon, Y. Guan, L. Y. Yam, W. Lim, J. Nicholls, W. K. Yee, W. W. Yan, M. T. Cheung, V. C. Cheng, K. H. Chan, D. N. Tsang, R. W. Yung, T. K. Ng, and K. Y. Yuen.** 2003. Coronavirus as a possible cause of severe acute respiratory syndrome. Lancet **361:**1319–1325.
59. **Pelham, H. R.** 1991. Multiple targets for brefeldin A. Cell **67:**449–451.
60. **Rota, P. A., M. S. Oberste, S. S. Monroe, W. A. Nix, R. Campagnoli, J. P. Icenogle, S. Penaranda, B. Bankamp, K. Maher, M. H. Chen, S. Tong, A. Tamin, L. Lowe, M. Frace, J. L. DeRisi, Q. Chen, D. Wang, D. D. Erdman, T. C. Peret, C. Burns, T. G. Ksiazek, P. E. Rollin, A. Sanchez, S. Liffick, B. Holloway, J. Limor, K. McCaustland, M. Olsen-Rasmussen, R. Fouchier, S. Gunther, A. D. Osterhaus, C. Drosten, M. A. Pallansch, L. J. Anderson, and W. J. Bellini.** 2003. Characterization of a novel coronavirus associated with severe acute respiratory syndrome. Science **300:**1394–1399.
61. **Schelle, B., N. Karl, B. Ludewig, S. G. Siddell, and V. Thiel.** 2006. Nucleocapsid protein expression facilitates coronavirus replication. Adv. Exp. Med. Biol. **581:**43–48.
62. **Stertz, S., M. Reichelt, M. Spiegel, T. Kuri, L. Martinez-Sobrido, A. Garcia-Sastre, F. Weber, and G. Kochs.** 2007. The intracellular sites of early replication and budding of SARS-coronavirus. Virology **361:**304–315.
63. **Tooze, J., S. Tooze, and G. Warren.** 1984. Replication of coronavirus MHV-A59 in sac- cells: determination of the first site of budding of progeny virions. Eur. J. Cell Biol. **33:**281–293.
64. **van der Hoek, L., K. Pyrc, M. F. Jebbink, W. Vermeulen-Oost, R. J. Berkhout, K. C. Wolthers, P. M. Wertheim-van Dillen, J. Kaandorp, J. Spaargaren, and B. Berkhout.** 2004. Identification of a new human coronavirus. Nat. Med. **10:**368–373.
65. **Vennema, H., G. J. Godeke, J. W. Rossen, W. F. Voorhout, M. C. Horzinek, D. J. Opstelten, and P. J. Rottier.** 1996. Nucleocapsid-independent assembly of coronavirus-like particles by coexpression of viral envelope protein genes. EMBO J. **15:**2020–2028.
66. **Wilson, L., P. Gage, and G. Ewart.** 2006. Hexamethylene amiloride blocks E protein ion channels and inhibits coronavirus replication. Virology **353:**294–306.
67. **Wilson, L., C. McKinlay, P. Gage, and G. Ewart.** 2004. SARS coronavirus E protein forms cation-selective ion channels. Virology **330:**322–331.
68. **Woo, P. C., S. K. Lau, C. M. Chu, K. H. Chan, H. W. Tsoi, Y. Huang, B. H. Wong, R. W. Poon, J. J. Cai, W. K. Luk, L. L. Poon, S. S. Wong, Y. Guan, J. S. Peiris, and K. Y. Yuen.** 2005. Characterization and complete genome sequence of a novel coronavirus, coronavirus HKU1, from patients with pneumonia. J. Virol. **79:**884–895.
69. **Woo, P. C., S. K. Lau, K. S. Li, R. W. Poon, B. H. Wong, H. W. Tsoi, B. C. Yip, Y. Huang, K. H. Chan, and K. Y. Yuen.** 2006. Molecular diversity of coronaviruses in bats. Virology **351:**180–187.
70. **Ye, Y., and B. G. Hogue.** 2007. Role of the coronavirus E viroporin protein transmembrane domain in virus assembly. J. Virol. **81:**3597–3607.